

Structure-Property Relationships Governing Membrane-Penetrating Behaviour of Complex Coacervates

Tiemei Lu, Xinyu Hu, Merlijn H. I. van Haren, Evan Spruijt,* and Wilhelm T. S. Huck*

Complex coacervates are phase-separated liquid droplets composed of oppositely charged multivalent molecules. The unique material properties of the complex coacervate interior favours the sequestration of biomolecules and facilitates reactions. Recently, it is shown that coacervates can be used for direct cytosolic delivery of sequestered biomolecules in living cells. Here, it is studied that the physical properties required for complex coacervates composed of oligo-arginine and RNA to cross phospholipid bilayers and enter liposomes penetration depends on two main parameters: the difference in ζ -potential between the complex coacervates and the liposomes, and the partitioning coefficient (K_p) of lipids into the complex coacervates. Following these guidelines, a range of complex coacervates is found that is able to penetrate the membrane of living cells, thus paving the way for further development of coacervates as delivery vehicles of therapeutic agents.

1. Introduction

The transport of biomacromolecules (peptides, proteins, DNA, or RNAs) across cellular membranes presents an important challenge in their development as therapeutic agents.^[1] The recent pandemic, but also rapid developments in new treatments against cancer, such as chimeric antigen receptors T-cell therapy, highlight the need for materials that aid in the transfection of cells.^[2] A wide range of materials based on cationic lipids, lipid nanoparticles, polymeric nanoparticles, and synthetic cationic polymers (e.g., polyethylenimine) has been developed to aid in the transport of agents across the cellular membrane.^[3] Among them, cationic lipid or polymer-based nanoparticles have been shown to yield universal and highly efficient cargo delivery, outperforming conventional methods based on viral vectors.^[4] However, the endocytosis of nanoparticles is a complex process, typically resulting in the formation of endosomal vesicles, which makes further release (endosomal escape) of active agents from

the nanoparticles a challenging part of the design of transfection materials.^[5]

Cell-penetrating peptides (CPPs) and polycationic polymers of bacterial origin can be conjugated with cargoes, such as proteins, peptides, and nucleic acids, and penetrate the membrane of cells to circumvent endocytosis and reach the cytosol directly, thereby enhancing the therapeutic effectiveness.^[6] These systems also have limitations; for example, CPPs often have low transfection efficiencies, as endocytosis and direct translocation routes coexist,^[7] and cargoes taken up by endocytosis must still escape from endosomes.^[8] Moreover, cargo conjugation to the CPPs or polymers is time-consuming and severely limits cargo versatility and delivery capacity.^[8]

Recently, Sun et al. found that pH- and redox-responsive peptide-based coacervate droplets of about 1 μm in diameter could enter living cells without becoming trapped in endosomes.^[9] Such coacervate droplets could act as emerging intracellular delivery vehicles,^[10] as a wide range of macromolecules can be recruited within the droplets, including small peptides, enzymes (up to 430 kDa), and messenger RNAs (mRNAs). Moreover, coacervates have a high loading capacity, allowing for the delivery of high payloads.^[9,10] Inspired by this report and our previous work that shows the interaction between coacervates and membranes can lead to membrane remodeling and endocytosis,^[11] we wished to explore whether complex coacervates could be developed into a new and broad class of transfection agents. We hypothesized that if the coacervate properties would be such that they can take up lipids by sequestration, then the coacervate could end up inside a membrane-bound compartment (liposome and cell) without an enclosing membrane and thus be able to release its contents.

In this work, we study the membrane penetration of complex coacervates in a model system under controlled conditions to explore the scope of “coacervate materials” that are capable of membrane penetration and obtain a better understanding of the underlying mechanism. Building on our previous work, we first engineered the coacervate materials to have a greater potential for the sequestration of lipids. For this, we replaced the small molecule spermine in our previous coacervates with oligoarginine, as oligoarginines are known to have favorable interactions with both phospholipid head groups and hydrophobic tails, which also underlies their membrane-penetrating properties. In contrast to our previous work, we observed that these coacervates crossed the membrane and that there appeared to be

T. Lu, X. Hu, M. H. I. van Haren, E. Spruijt, W. T. S. Huck
Institute for Molecules and Materials
Radboud University
Heyendaalseweg 135, Nijmegen 6525 AJ, the Netherlands
E-mail: e.spruijt@science.ru.nl; w.huck@science.ru.nl

 The ORCID identification number(s) for the author(s) of this article can be found under <https://doi.org/10.1002/smll.202303138>

© 2023 The Authors. Small published by Wiley-VCH GmbH. This is an open access article under the terms of the Creative Commons Attribution License, which permits use, distribution and reproduction in any medium, provided the original work is properly cited.

DOI: 10.1002/smll.202303138

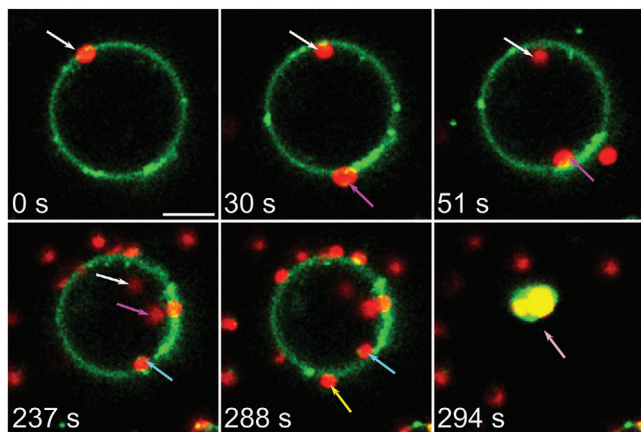


Figure 1. Penetration of R_{10} /tyRNA coacervates (red, labelled with polyA₁₅-Cy5, marked with arrows) into liposomes (POPC_{0.4}/cholesterol_{0.1}/PG_{0.5} liposome (green, labelled with DOPE-Atto 488). The scale bar represents 10 μm .

no membrane enclosing these coacervates after they crossed. Extensive variations in the composition of the coacervates and the liposomes allowed us to draw general conclusions about the key requirements for membrane penetration: a moderate attraction between the coacervate surface and the liposome facilitates the initial contact, while a sufficiently high lipid partition coefficient of the coacervate materials ensures that the lipid bilayer does not envelop the coacervates, but the lipids contacting the coacervates are taken up allowing the coacervates to cross the lipid bilayer as a membrane-permeating material. Finally, we demonstrate that coacervates that meet these requirements are capable of crossing the membranes of living cells, opening up a new direction for further study of this promising class of transfection materials.

2. Results and Discussion

2.1. Complex Coacervates can Cross Liposome Bilayers

As shown in **Figure 1**; Movie S1 (Supporting Information), coacervates composed of oligoarginine (R_{10} , 2.7 kDa) and torula yeast RNA (tyRNA), labeled with fluorescently labeled DNA oligonucleotides (polyA₁₅-Cy5), crossed the membrane of liposomes composed of 40 wt.% POPC, 10 wt.% cholesterol, and 50 wt.% negatively charged PG, labeled with 0.17 wt.% DOPE-Atto 488. There appears to be no clear membrane around these coacervates once inside the liposomes (Figure S1, Supporting Information), in contrast to our previous results for complex coacervates composed of spermine and polyU RNA, which wetted the liposomes or were engulfed by endocytosis.^[11] Over the course of several minutes, more and more R_{10} /tyRNA coacervates penetrated the membrane of the liposome, until it eventually burst, forming an aggregate of lipids and coacervates (294 s). Notably, the diameter of the liposome decreased by 3.8 μm prior to bursting and the coacervates that penetrated the liposome showed a slightly enhanced fluorescence signal of DOPE-Atto 488 (Figure S2, Supporting Information), which could be an indication that the coacervates take up lipids from the liposome.

After the coacervates penetrated the membrane of the liposomes, some coacervates remain attached to the inner leaflet of

the membrane due to the electrostatic attraction between the coacervate and the liposome membrane. However, the coacervates are clearly inside the liposome, as observed from confocal imaging along three orthogonal planes (Figure S3, Supporting Information). The translational movement of the coacervates is independent of that of the liposome after penetration (Movie S2, Supporting Information), and some coacervates were found to have detached from the membrane (Figure S3a–c).

2.2. Investigating the Composition of Complex Coacervates

Intrigued by the above findings, we wished to explore the general material properties that govern the transport of complex coacervates across lipid bilayers. R_{10} is an arginine-rich oligopeptide resembling cell-penetrating peptides, which are lysine- and arginine-rich cationic oligopeptides (5 to 35 amino acids) and exhibit the rare ability to cross the cell membrane. These arginine-rich peptides are used to deliver cargoes (e.g., proteins and nucleic acids) to cells and tissues.^[12] The membrane translocation abilities of oligoarginines in living cells depend on their chain length and charge density.^[13] Thus, we prepared complex coacervates containing tyRNA and oligoarginines with a range of different lengths (R_5 , R_{10} , R_{20} , and R_{40} , see SI Materials), as well as oligopeptides with different charge distributions, ((RRASL)₃ and (RGRGG)₅, see Supporting Information Materials). We labelled these coacervates with fluorescein-labelled R_{10} , ((RRASL)₃, (RGRGG)₅ (R_{10} -FAM, (RRASL)₃-FAM, (RGRGG)₅-FAM), and polyA₁₅-Cy5, respectively. These coacervates exhibited a range of surface charges (see Table S1, Supporting Information and **Figure 2a** for their ζ -potentials). Subsequently, the coacervates were mixed with liposomes of opposite charge (POPC_{0.4}/cholesterol_{0.1}/PG_{0.5} or POPC_{0.7}/cholesterol_{0.1}/DOTAP_{0.2}). The absolute differences in ζ -potential ($\Delta\zeta$, absolute values of the ζ -potential of coacervates – liposomes) are shown in **Figure 2b**.

Coacervates containing short R_5 (ζ -potential –14.4 mV) formed wetting morphologies after mixing with liposomes (Figure 2c), whereas coacervate droplets with R_{10} or R_{20} (ζ -potential 12.5 and 23.0 mV, respectively) penetrated and entered the liposomes (Figure 2d,e). At the same time, lipids partitioned into these coacervates upon crossing the membrane (overlapping red/green fluorescence in the composite images). However, when the length of the oligoarginines in the coacervate was increased further to 40 (Figure 2f), the droplets tended to adhere to the surface of the liposome, and only a few droplets penetrated the membrane of the liposome. This could be caused by the fact that R_{40} /tyRNA coacervates have a high ζ -potential (40.3 mV), which results in strong electrostatic interactions (high $\Delta\zeta$, Figure 2b) between the coacervates and the liposome membrane.^[11] The importance of ζ -potential was further confirmed when studying the ((RRASL)₃/tyRNA and (RGRGG)₅/tyRNA coacervates (ζ -potential –3.1 and 5.8 mV, respectively), which both did not penetrate the membrane of liposomes; they exhibited partial wetting or endocytosis into the liposomes (Figure 2g,h).

After investigating the role of oligoarginine peptides in coacervates, we wanted to examine the role of the nucleic acid component of our coacervates, particularly whether tyRNA was required

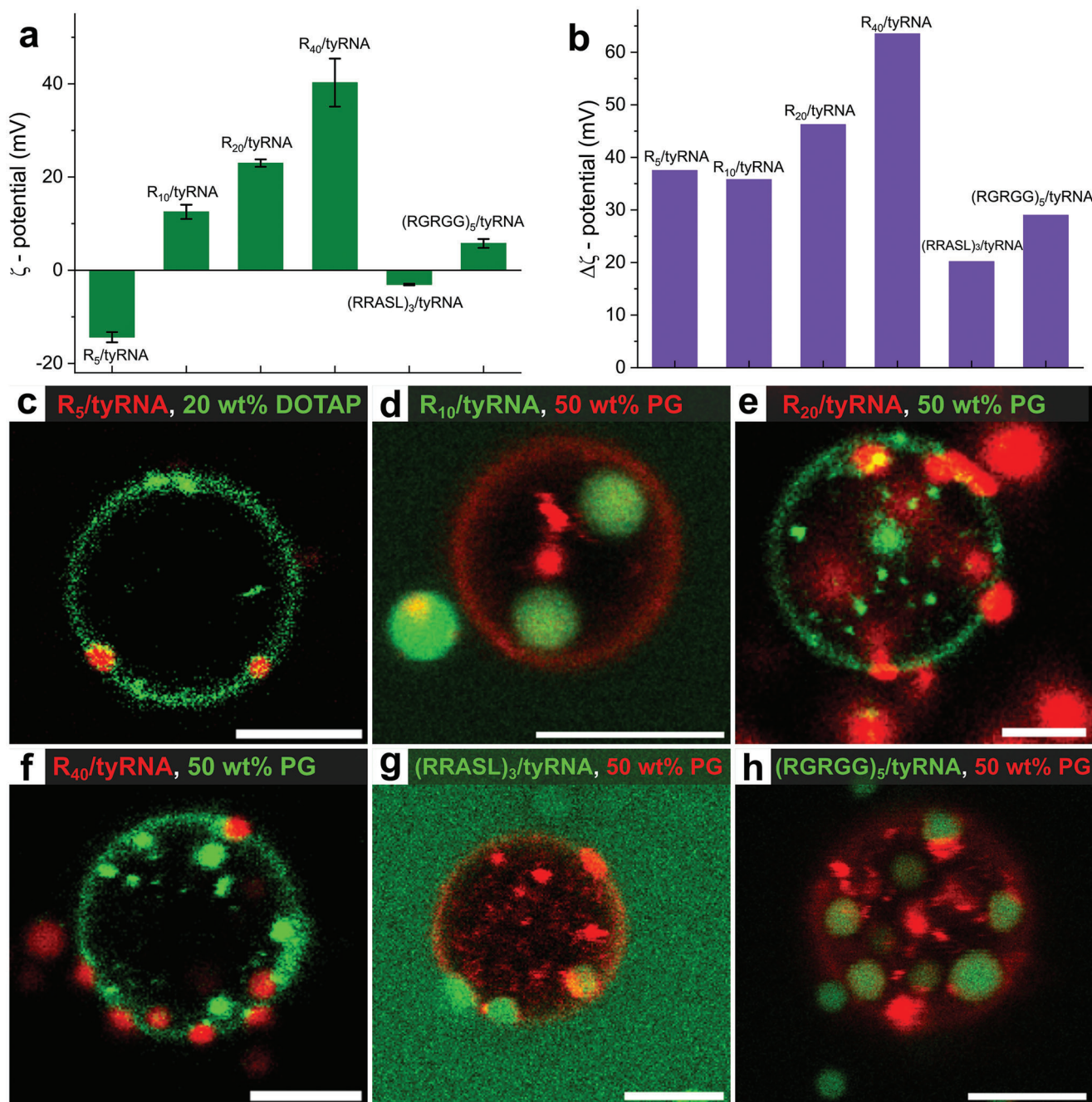


Figure 2. a) ζ -potentials of different lengths or charge densities of oligoarginine peptide coacervates; b) $\Delta\zeta$ of oligoarginines coacervates and liposomes; c–h) composite images of oligoarginine peptide coacervates mixed with oppositely charged liposomes. The red (c,e,f) coacervates were labelled with polyA₁₅-Cy5, and green (d,g,h) coacervates were labelled with R_{10} -FAM, $(RRASL)_3$ -FAM, and $(RGRGG)_5$ -FAM, respectively. The green (c,e,f) and red (d,g,h) liposomes were labelled with DOPE-ATTO 488 and DOPE-ATTO 655, respectively. Scale bars represent 5 μ m.

for the membrane penetration. Thus, we further modulated the properties of coacervates by forming complex coacervates between the various oligoarginines (R_5 , R_{10} , R_{20} , and R_{40}) and ATP, RNA (polyA), and short single-stranded DNA (ssDNA) sequences $(ACTG)_2$, $(ACTG)_5$, and $(ACTG)_{15}$. The ζ -potentials of these coacervates were found to increase as the length of oligoarginine increased, as shown in Table S1 (Supporting Information) and **Figure 3a**. The resulting coacervates were then mixed with lipo-

somes of opposite charge (ζ -potential range from -23.2 mV to 23.1 mV), and the $\Delta\zeta$ -potentials are shown in **Figure 3b**.

Coacervates containing short R_5 and ssDNA $(ACTG)_5$ (red) showed partial wetting and some endocytosis when mixed with oppositely charged liposomes (green) (**Figure 3c**), in agreement with our findings for R_5 /tyRNA in **Figure 2**. Coacervates with a small multivalent anion, such as ATP, also ended up inside oppositely charged liposomes via endocytosis (**Figure 3d**). However,

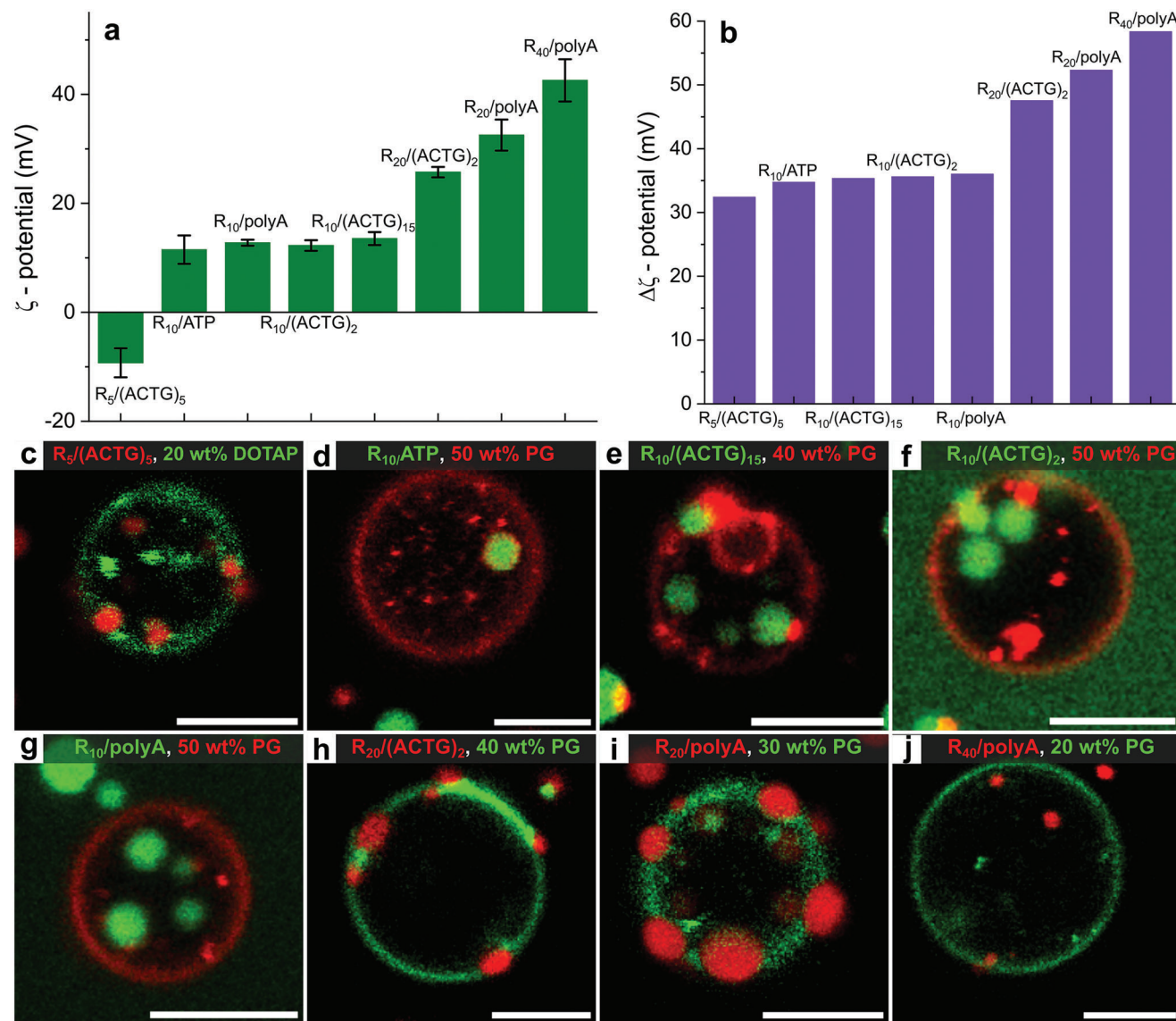


Figure 3. a) ζ -potentials of different types of coacervates; b) $\Delta\zeta$ of coacervates and liposomes; c–j) composite images of RNA or ssDNA coacervates mixed with positively (c) or negatively (d–j) charged liposomes. The green and red coacervates and liposomes represent labeling R_{10} -FAM and polyA₁₅-Cy5, DOPE-ATTO 488 and 655, respectively. Scale bars represent 5 μm .

all coacervates containing R_{10} and longer oligonucleotides (RNA (tyRNA, polyA) or ssDNA ((ACTG)₂ and (ACTG)₁₅) could penetrate the membrane of liposomes (Figure 3e–g), coinciding with indications of lipid partitioning into the coacervates (overlapping red/green fluorescence).

In general, the ζ -potentials of the coacervates obtained after mixing RNA or ssDNA with R_{20} and R_{40} were higher than those obtained after mixing with R_{10} (Figure 3a), resulting in stronger electrostatic interactions with membranes containing charged lipids, and a tendency to partial wetting. Therefore, we reduced the PG concentration to 40 wt.% or 20 wt.%. $R_{20}/(\text{ACTG})_2$ and R_{20}/polyA coacervates still showed partial wetting on more weakly charged membranes (Figure 3h,i). However, after mixing the R_{40}/polyA coacervates with PG 20 wt.% liposomes, we again observed coacervates penetrating the membrane of the liposomes

(Figure 3j). Notably, the size of R_{40}/polyA coacervates in Figure 3j is smaller than the $R_{20}/(\text{ACTG})_2$ and R_{20}/polyA coacervates that showed partial wetting in Figure 3h,i, which could play a role in coacervates penetrating the liposome membrane.

In short, these experiments show that in order to obtain membrane-penetrating coacervates, tyRNA is not specifically required. Indeed, coacervates formed with (ACTG)₂, (ACTG)₁₅, or RNA (polyA) can also penetrate the membrane of liposomes. Moreover, analysis of the ζ -potential difference suggested that moderate electrostatic attraction facilitates membrane penetration, whereas strong electrostatic attraction leads to the wetting of coacervates on the surface of liposomes.

In addition to studying the effect of polyanions (ATP, RNA, or ssDNA), we wished to understand whether the penetration was mainly due to the presence of oligoarginines. We,

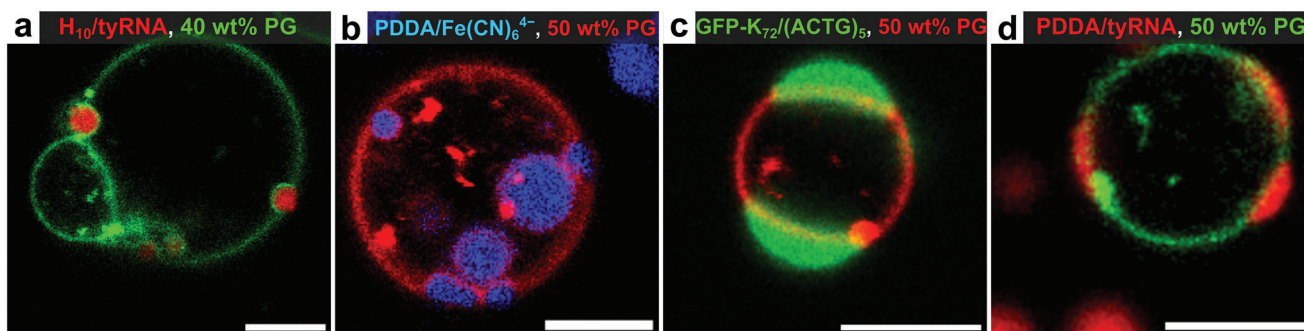


Figure 4. a–d) Composite images of the interaction of POPC/PG liposomes and different types of coacervates. The red (a,d) and blue (b) coacervates represent labeling with polyA₁₅-Cy5 and free pyranine dye, respectively. The green coacervates (c) come from the same color as the GFP-K₇₂. The green and red liposomes represent labeling with DOPE-ATTO 488 and 655, respectively. Scale bars represent 5 μm.

therefore, produced coacervates containing the positively charged oligopeptide poly-L-histidine H₁₀ (see Supporting Information Materials), polyelectrolyte poly(diallyl dimethylammonium) chloride (PDDA), and a lysine-rich intrinsically disordered protein GFP-K₇₂. H₁₀/tyRNA, PDDA/Fe(CN)₆⁴⁻, PDDA/tyRNA, and GFP-K₇₂/(ACTG)₅ coacervates all showed positive ζ-potentials (Table S1, Supporting Information) and were mixed with negatively charged PG (40 wt.% or 50 wt.%) liposomes. However, we did not observe any example of membrane penetration by these coacervates. Instead, the coacervates containing H₁₀, PDDA, and GFP-K₇₂ showed either partial wetting (Figure 4a,c), clear endocytosis (Figure 4b), or complete wetting (Figure 4d). This strongly suggests an important role for oligoarginines in the coacervates, although we also note that the Δζ are 44.4, 28.9, 41.3, and 55.7 mV, respectively, whereas we observed the most efficient membrane penetration

for oligoarginine-based complex coacervates at Δζ ≈ 35 mV (Figure 3).

2.3. Investigating the Effect of Membrane Composition

Given the potential importance of the ζ-potential difference, we studied the interaction of oligoarginine-containing coacervates with liposomes of different charges. R₁₀/tyRNA coacervates were mixed with negatively charged liposomes which contain different concentrations of POPG (PG) (Table S1 and Figure S4, Supporting Information). As shown in Figure 5a–c, the electrostatic interaction between coacervate droplets and liposomes increased with the concentration of PG. Without PG (0 wt.%) (Figure 5a), coacervate droplets only touch the surface of liposomes. As the PG fraction increased, we first observed partial wetting and partial penetration (30 wt.%, Figure 5b), followed by complete

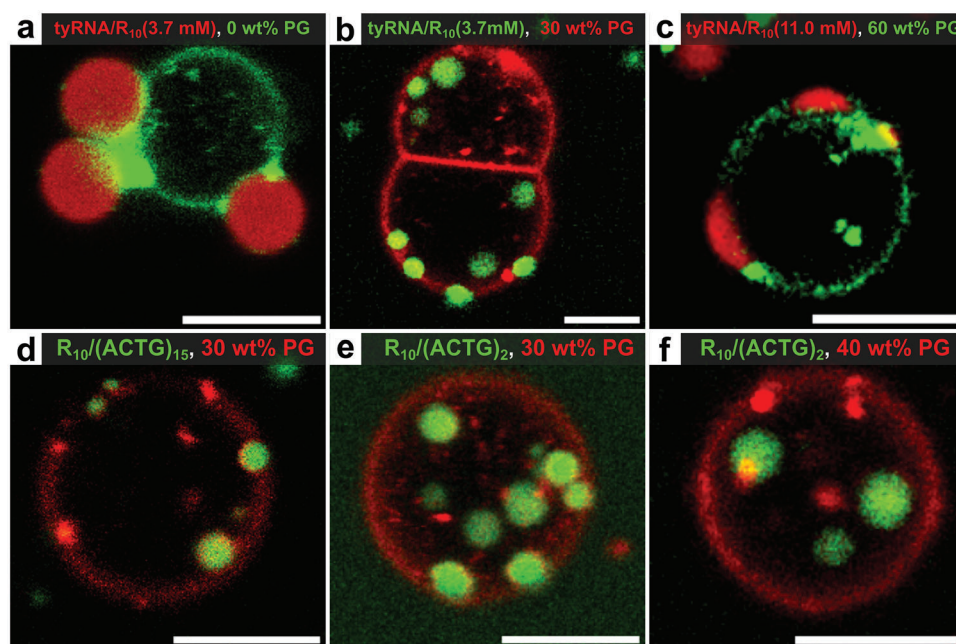


Figure 5. Interaction of POPC/PG liposomes and a–c) R₁₀/tyRNA, d) R₁₀/(ACTG)₁₅, e,f) R₁₀/(ACTG)₂ coacervates for different PG fractions. The red and green coacervates represent labeling with polyA₁₅-Cy5 and R₁₀-FAM, respectively. The green and red liposomes represent labeling with DOPE-ATTO 488 and 655, respectively. Scale bars represent 5 μm.

penetration (50 wt.%, Figure 2d), and ultimately spreading of coacervates into thin lenses that deform the membrane (60 wt.%, Figure 5c), in agreement with our observations in Figure 3h,i.

A similar trend was observed for $R_{10}/(\text{ACTG})_{15}$, $R_{10}/(\text{ACTG})_2$, R_{20}/tyRNA , and PDDA/tyRNA coacervates (Figure 5d–f; Figure S5, Supporting Information). When the concentration of PG was reduced to 30 wt.%, partial wetting, and endocytosis-like morphologies were observed for $R_{10}/(\text{ACTG})_{15}$ (Figure 5d), while $R_{10}/(\text{ACTG})_2$ coacervates showed both endocytosis and membrane penetration (Figure 5e). When the PG concentration was increased to 40 wt.%, both types of coacervates always penetrated the liposome membrane, and we observed lipid partitioning into the coacervates (overlapping red/green fluorescence in Figure 5f).

2.4. A Possible Mechanism for Membrane Penetration by Complex Coacervates

The results thus far point to a role for the ζ -potential difference ($\Delta\zeta$) in facilitating the interaction between coacervates and membranes. For moderate attraction, coacervates could be taken up by endocytosis, as we observed in our previous work for spermine/polyU coacervates, or penetrate the membrane, as we observed here for oligoarginine-containing complex coacervates. The presence of oligoarginines of intermediate length (R_{10} , R_{20}) seems to determine the membrane penetration potential, but this does not yet explain how coacervates cross the membrane without endocytosis. Motivated by the observed decrease in the size of liposomes and the presence of lipid fluorescence inside the coacervates after they crossed the membrane, we hypothesize that the ability to sequester lipids in the coacervates is an important requirement that governs the membrane penetration by coacervates. Coacervates are known for their ability to sequester a wide range of guest molecules, including lipids,^[14] and even intact liposomes (100 nm).^[15] To support our hypothesis that lipid partitioning correlates with membrane penetration, we measured the partitioning coefficients (K_p) of DOPE-ATTO 655 lipids in all the coacervates studied so far (see Table S1 and Figure S6, Supporting Information).

The broad range of obtained K_p values, ranging from 0 (non-partitioning) to 360 (strong partitioning), reflects the strongly varying levels of hydrophobicity of the coacervates under study.^[16] For example, complex coacervates without oligoarginine or histidine show K_p values in the range of 0 to 10 (Figure S6a,b, Supporting Information), indicating that lipids are hardly taken up by these coacervates, whereas coacervates containing oligoarginine or histidine exhibit K_p values of 21 up to 360 (Figure S6c–f, Supporting Information). Typically, shorter oligoarginines ($N < 10$) or peptides with a lower charge density due to the presence of other non-charged amino acids (e.g., (RGRGG)₅) have a lower K_p . Arginine and lysine differ in their ability to form cation- π and π - π interactions with the nucleobases in RNA and DNA. This results in the formation of more hydrophobic and viscous coacervates formed by oligoarginine and oligonucleotides than lysine-rich peptides and oligonucleotides,^[17] and explains why the GFP- $K_{72}/(\text{ACTG})_5$ coacervates have a K_p of only 5.2.

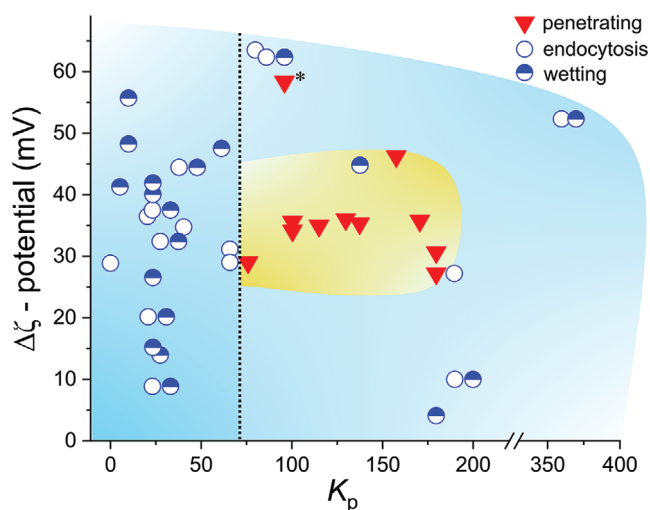


Figure 6. Morphological state diagram of the interplay between complex coacervates and liposomes as a function of their absolute ζ -potential difference ($\Delta\zeta$) and the coacervate lipid partition coefficient K_p . *Denotes a special case of R_{40}/polyA coacervates that were significantly smaller (average diameter $< 1 \mu\text{m}$) than most other coacervate samples and were found to penetrate the liposome membrane despite a strong surface attraction (Figure 3j), as discussed in the main text.

To summarize the main parameters that govern the interaction of coacervates with membranes, we mapped the various observed morphologies (i.e., i) membrane penetration (e.g., Figure 2d), ii) endocytosis (e.g., Figures 3d,4b), and iii) partial or complete wetting on the surface of liposomes (e.g., Figure 4c,d) onto a parameter diagram containing the $\Delta\zeta$ and K_p values. **Figure 6** shows that membrane penetration never occurs for coacervates with a K_p value below ≈ 75 . Instead, partial wetting or endocytosis was found for all coacervates, irrespective of the ζ -potential difference (blue-shaded region, on the left of the dotted line). For sufficiently high K_p values (above 75), membrane penetration by complex coacervates is possible. The criteria for the ζ -potential difference are less strongly defined, but membrane penetration by complex coacervates was primarily observed for moderate ζ -potential differences, between 25 and 45 mV (yellow-shaded area). In this region, electrostatic attraction facilitates contact between the coacervates and liposomes surfaces, while lipid partitioning allows the complex coacervates to translocate the lipid bilayer without forming a new membrane. It is possible that the coacervates are partly covered by a membrane as they start entering the liposomes, analogous to what happens during endocytosis, after which the lipids partitioned into the coacervate. However, time-lapse microscopy experiments in which we captured the membrane penetration process did not show lipids present at the surface of the coacervates as they entered the liposome. Therefore, we conclude that the lipid partitioning takes place on a short timescale compared to the complete membrane crossing.

To further support our proposed mechanism, we did an additional experiment, namely, pre-incubation of coacervates with lipids (Figure S7, Supporting Information). As discussed above, we hypothesize that the lipid partitioning constant K_p is a major driving force for the coacervates penetrating the membrane of liposomes. When lipids partition into the coacervates, the

interaction between coacervates and liposomes will change. Coacervates that are close to saturation will not be able to take up enough lipids to penetrate the liposomal membrane. From Figure S7a (Supporting Information), it can be observed that the interaction of $R_{10}/(\text{ACTG})_2$ coacervates that are previously incubated with lipids interact different from non-incubated coacervates: in contrast to the previously observed penetrating behavior (e.g., Figure 3f, Figure 5f) coacervates now proceed from no contact ($t = 0$ s), followed by attaching ($t = 390$ s) to final spreading on the surface of liposome ($t = 890$ s). The difference in coacervate-liposome interaction can be made more explicit by comparing the composite fluorescence images (Figure S7b,c). Coacervates incubated with lipids only showed wetting morphologies after 4740 s (indicated by the white arrow, Figure S7b, Supporting Information). In contrast, non-incubated coacervates were observed to penetrate the liposome (indicated by pink arrows) or disrupt the liposomes and form aggregates (indicated by the yellow arrow) after 6600 s (Figure S7c, Supporting Information). The above results indicate that after incubating the coacervates with lipids and mixing them with liposomes, the capability of the coacervates to sequester lipids is reduced, and the interaction between coacervates and liposomes is weakened with reduced hydrophobic interactions.

As the K_p is the main parameter for the coacervate to penetrate the membrane of the liposome, we tested one type of simple coacervate, FFsFF, which composition is quite different from the complex coacervates and with much higher K_p (Table S1, Supporting Information). We found that these small-sized coacervates can also penetrate the membrane of liposomes (Figure S8, Supporting Information).

In addition, the mechanism that we proposed also suggests that membrane remodeling and transient pore formation in the liposome membrane could be expected.^[18] To study leakage of the membrane we measured the diffusion of R_{10} -FAM molecules from the external solution into the liposomes upon interaction with coacervates. Figure S9a (Supporting Information) shows the increase in fluorescence intensity over time. In all experiments the fluorescence intensities go up over time, suggesting that coacervates change the permeability of the liposomes upon their interaction and allow fluorescent molecules to leak in. This is also apparent in the example composite images of coacervates interacting with a liposome (Figure S9b, Supporting Information). Several R_{10} -FAM/ $(\text{ACTG})_2$ coacervates adhered to the liposome membrane ($t = 720$ s), and the fluorescence intensity inside the liposome was significantly increased at $t = 2020$ s. As a control, we studied the interaction of R_{10} -FAM into the liposomes in the absence of coacervates. In this case, the fluorescence intensity did increase, but significantly less than in the presence of oligoarginine-containing coacervates (Figure S9a,c, Supporting Information).

According to our mechanistic hypothesis, the ζ -potential difference ($\Delta\zeta$) and the partitioning coefficient (K_p) of lipids into the complex coacervates are the two main parameters for penetration. This simplified model did not take other parameters into account, for example, the fluidity of the liposome membrane. As cholesterol can change the fluidity of GUV membranes,^[19] we increased the cholesterol (CH) concentration to 20 wt.% in liposomes and then mixed these with two different types of coacervates (R_{10}/tyRNA and R_{40}/polyA). As shown in Figure S10 (Sup-

porting Information), the increase in CH concentration did not markedly change the behaviour of coacervate droplets penetrating the membrane of liposomes. Based on these experiments, we therefore do not see a major role of membrane fluidity in the penetration of membranes by coacervates.

2.5. Lipid-Sequestering Complex Coacervates can Enter Cells

All experiments thus far have involved simple liposomes. To demonstrate that the mechanism of membrane penetration is general and can be developed for cell transfection materials, we studied whether the complex coacervates could also penetrate cell membranes. Complex coacervates R_{10}/tyRNA and $R_{10}/(\text{ACTG})_2$, prepared in cell culture medium (DMEM), were added to NIH/3T3, HELA, and MCF-7 cells and incubated for one hour, after which the cells were extensively washed with cell culture medium to remove any complex coacervates that were not taken up.

As shown in Figure 7a,b; Figure S11 (Supporting Information), complex coacervates were found inside all three types of cells (R_{10} -FAM channel). The number of coacervates varied from several to tens of coacervates, and their sizes (1–3 μm) were in good agreement with the sizes of the as-prepared coacervates. Coacervates in the cells were mobile and all located in the cytosol and without apparent colocalization with other intracellular structures or wetting to the cell membrane (Movie S3, Supporting Information). Z-stack imaging and time-resolved fluorescence microscopy were used to confirm that R_{10}/tyRNA coacervates had indeed entered NIH/3T3 cells (Figure S12a and Movie S4, Supporting Information). Finally, R_{10}/tyRNA coacervates that were prepared with the same buffer as was used for the liposomes (Figures 1–5) and added to NIH/3T3 cells also ended up inside the cells (Figure S13, Supporting Information). This indicates that the buffer solution used to prepare the coacervates does not affect the properties of the cells.

Since R_{10} is a cell-penetrating peptide, a comparative set of experiments was done. When R_{10} -FAM alone (no coacervate formation) was incubated with NIH/3T3 cells for one hour after and rinsed, an increased fluorescence intensity corresponding to R_{10} -FAM was found in the cell cytoplasm (Figure S14a–c, Supporting Information), which is consistent with CPPs studies.^[13] However, only irregular-shaped aggregates, presumably formed by R_{10} with complexed with cytoplasmic RNAs, were observed inside the cells (Figure S14a–c, Supporting Information, R_{10} -FAM channel) and, contrary to cells that were incubated with R_{10}/tyRNA and $R_{10}/(\text{ACTG})_2$ coacervates, no coacervate droplets could be seen in the cells. To further prove that the complex coacervates penetrate the cell membrane and enter the cells as intact, droplet-like objects, we used poly A_{15} -Cy5 to label the R_{10}/tyRNA coacervates. We found that the fluorescently labeled RNA colocalized with the coacervate droplets inside the cells (Figure 7c, Z-stack image and video in Figure S12b; Movie S5, Supporting Information). However, when incubating the cells with only poly A_{15} -Cy5 without coacervates, no fluorescence could be observed inside the cells (Figure S14d, Supporting Information), suggesting that R_{10}/tyRNA coacervates entered the cells as a single droplet-like object.

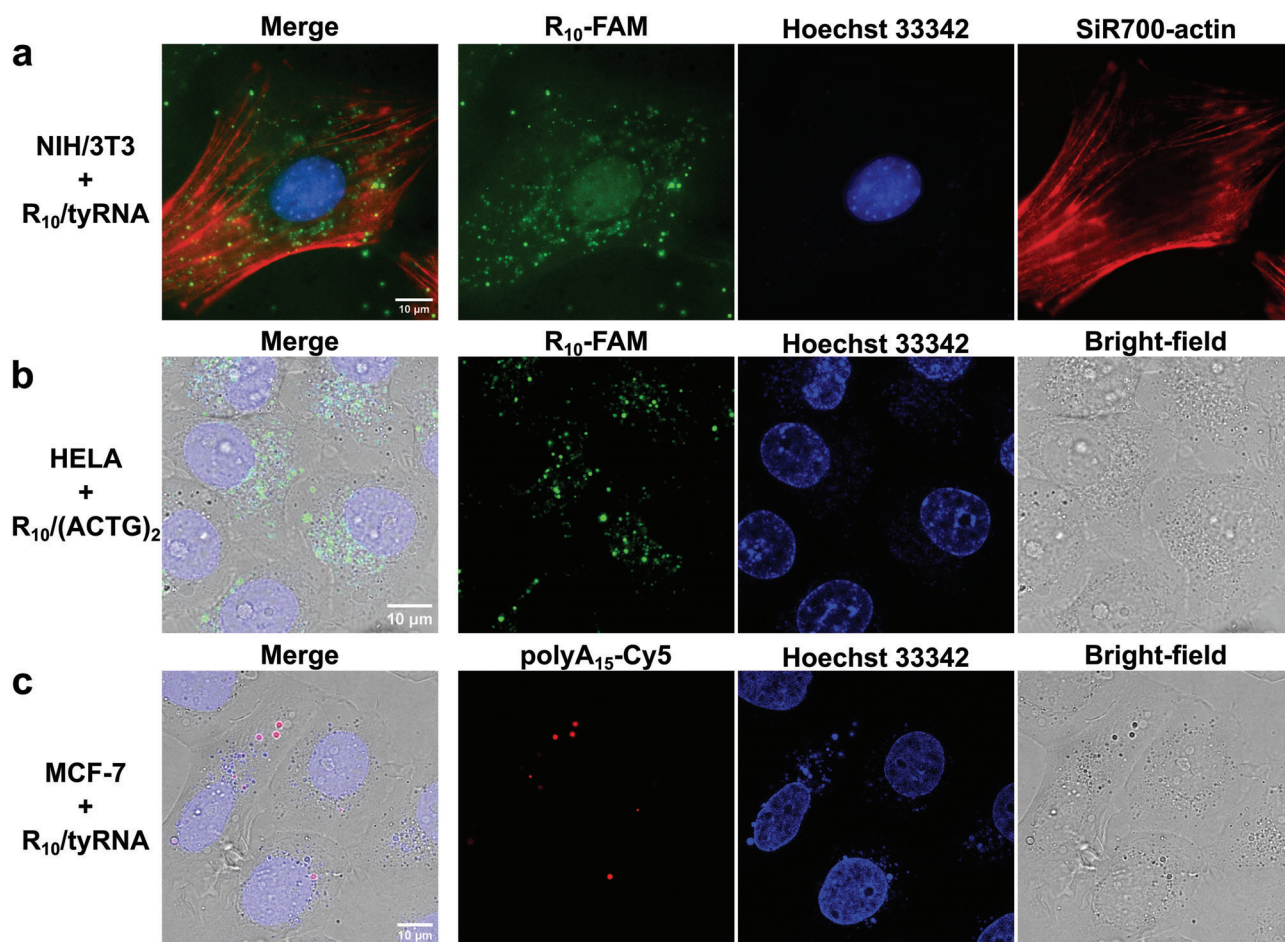


Figure 7. Merged and different channel images of coacervates a) $R_{10}/tyRNA$ (green, labeled with R_{10} -FAM), b) $R_{10}/(ACTG)_2$ (green, labeled with R_{10} -FAM), and c) $R_{10}/tyRNA$ (red, labeled with $polyA_{15}$ -Cy5) penetrating living cells NIH/3T3, HELA, and MCF-7 respectively. The living cell nuclei of NIH/3T3, HELA, and MCF-7 were labeled with Hoechst 33 342 (blue), and the membrane of NIH/3T3 in a) was labeled with SiR700-actin (red).

3. Conclusion

We found that complex coacervates containing oligoarginines of intermediate length and various oligonucleotides could penetrate the membrane of liposomes, making these droplets potentially interesting as candidates for a novel and broad class of transfection agents. To gain insights into a possible mechanism, we systematically studied the interactions between complex coacervates and liposomes containing different charge densities. We found that the ability of coacervates to sequester lipids (as quantified by the K_p) determines their ability to penetrate lipid membranes. The attractive electrostatic interactions ($\Delta\zeta$) between coacervate and lipids help form the initial contact necessary for this process to occur. Moreover, once coacervates take up lipids, the phospholipid bilayer of the liposome rearranges, resulting in a smaller liposome.

For coacervates with a low K_p (<75), the electrostatic surface interactions dominate after mixing coacervates and liposomes, which will lead to the formation of wetting or endocytosis morphologies. In contrast, coacervates with a sufficiently high K_p (>75), were able to take up lipids when contacting the liposome membrane and showed the highest potential to penetrate

the membrane. Interestingly, all these complex coacervates contained oligoarginines, which are known for their cell-penetrating properties. They are usually more hydrophobic than peptides with a low density of arginines, poly-lysine, or other positively charged coacervates, as reflected here by their higher K_p .

Finally, we found that complex coacervates that can penetrate the liposomes can also be observed in different living cells. As a next step, the coacervates can be designed as transfection agents to load and deliver RNA, enzymes, or drugs into living and synthetic cells. In addition, our findings are built on directly measurable parameters that relate to coacervate material properties, such as the partition coefficient K_p , enabling the prediction of the transfection potential of other coacervates.

4. Experimental Section

See supporting information for detailed materials and experimental section.

Preparation of Liposomes and Coacervates: The emulsion transfer method was used to prepare liposomes, described in previous work.^[11] The method for preparing complex coacervates also has been reported.^[11]

Incubation of Coacervates with Cells: The NIH/3T3 (fibroblast cell), MCF-7 (breast cancer cell), and HELA (cervical cancer cell) cells were grown in μ -slide 18 well glass bottom (ibidi, 81 817, without modification) and the growth medium was supplied with $2.5 \mu\text{g mL}^{-1}$ Hoechst 33 342 (final concentration) for 1 h at 37°C to label nucleus. Cells were washed once with culture medium (DMEM) after staining and then stained with $1 \mu\text{M}$ SiR700-actin (spirochrome, SC013) in culture medium for 30 mins at 37°C to label membrane. After labeling the living cell nuclei and membrane, Complex coacervates R_{10} /tyRNA (labeled with R_{10} -FAM or polyA₁₅-Cy5) and R_{10} /(ACTG)₂ (labeled with R_{10} -FAM), were then separately added to the cells. After 1 h of incubation of coacervates with living cells at 37°C , the cells and coacervates mixture were then washed four times with DMEM buffer solution to clean the droplets distributed around the cells without entering them and then observed using Sp8x confocal microscope (37°C) or Nikon Ti2-E microscope.

Confocal Microscopy Experiments: The samples of interaction between coacervates and liposomes for the microscopy experiments were prepared by the same method described before.^[11] Samples of interaction between coacervates and living cells (at 37°C) for the microscopy experiments were prepared as described above. Images and videos were obtained using a Leica TCS Sp8X confocal microscope equipped with HyDs and PMTs detectors and a pulsed white light laser. HC PL APO CS2 $40\times/1.10$ (water) and $100\times/1.40$ (oil) objectives were used. Samples were visualized by excitation of 405 nm (pyranine), 488 nm (R_{10} -FAM), 501 nm (ATTO-488), 649 nm (ATTO-655, Cy5), and 690 nm (SiR700-actin). For the samples of R_{10} /tyRNA coacervates and NIH/3T3 cells, the images and Z-stack video were also obtained by using a Nikon Ti2-E microscope with Perfect Focus System and CFI ($100\times$ oil objective). Excitation was performed using a SpectraX LED engine (Lumencor) and 488 nm, 561 nm, and 640 nm lasers.

Lipid Partitioning Experiments: The complex and simple coacervates were prepared first, and then added $0.5 \mu\text{L}$ of DOPE-ATTO 655 lipid chloroform solution to each coacervates solution ($20 \mu\text{L}$) separately. After 30 mins of incubation, fluorescence images was taken by Sp8x confocal microscopy. Images were probed and analyzed with MATLAB 2021 Image Processing Toolbox. An automatic threshold was determined, and objects smaller than 50 pixels were excluded from the analysis, and the areas and mean intensities for droplets above the threshold were extracted. The mean dilute phase intensity was calculated from the image with all droplet intensities subtracted. Subsequently, the partitioning coefficients (K_p) were then calculated by the following equation:^[16b] $K_p = (I_{\text{coa}} - I_b) / (I_d - I_b)$, where I_{coa} , I_b , and I_d are the intensities of a coacervate, a blank solution, and the dilute phase surrounding the coacervate droplets, respectively.

Pre-Incubation of Coacervates with Lipids: Before mixing the coacervates with the liposomes, $1 \mu\text{L}$ of lipids in chloroform with the same composition as the POPC/POPG/cholesterol liposomes was incubated for 1 h with $20 \mu\text{L}$ of the R_{10} /(ACTG)₂ coacervates, after which the coacervates were mixed with the liposomes. The images were recorded by Sp8X confocal.

Leakage Assay: The R_{10} -FAM labelled R_{10} /(ACTG)₂ coacervates were added into POPC_{0.4}/cholesterol_{0.1}/POPG_{0.5} liposomes solution, and then a video, which was composed of a series of images, was recorded on a Sp8X confocal. The interval time of detection was 10 s. For comparison, the exact same amount of R_{10} -FAM was added into the same buffer solution as R_{10} /(ACTG)₂ coacervates, followed by mixing the R_{10} -FAM buffer solution with the liposomes. Then, a video with an interval time of 10 s was also recorded. Afterward, the data points of fluorescence intensity increasing in liposomes or decreasing in coacervate(s) over time were obtained from videos by analysis in Matlab (SI 2.9: Quantitative liposome fluorescence analysis).

Supporting Information

Supporting Information is available from the Wiley Online Library or from the author.

Acknowledgements

This work was supported financially by a Spinoza Grant of the Netherlands Organization for Scientific Research (NWO), the International Human Frontier Science Program Organization (HFSP) via award RGY00062/2022, and a Scholarship from the China Scholarship Council (CSC). The authors would like to thank Alain A. M. André for purifying GFP-K72; Dr. N. Amy Yewdall and Dr. Oliver R. Maguire for helpful writing suggestions and feedback; Dr. Yue Sun and Prof. Ali Miserez for the helpful discussions.

Conflict of Interest

The authors declare no conflict of interest.

Author Contributions

T.L., E.S., and W.T.S.H. conceived and designed the project. T.L. carried out the experiments and data analysis. X.H. cultured labelled cells and incubated coacervates and cells. M.H.I.vH wrote the MATLAB scripts, assisted with fluorescence measurements, and expressed and purified GFP-K72. T.L., E.S., and W.T.S.H. wrote the manuscript with input from all co-authors.

Data Availability Statement

The data that support the findings of this study are available in the supplementary material of this article.

Keywords

complex coacervates, delivery vehicles, liposomes, partitioning coefficient

Received: May 2, 2023

Published online:

- [1] a) L. Wang, N. Wang, W. Zhang, X. Cheng, Z. Yan, G. Shao, X. Wang, R. Wang, C. Fu, *Signal Transduct Target Ther* **2022**, 7, 48; b) V. Y. Berdan, P. C. Klauser, L. Wang, *Bioorg. Med. Chem.* **2021**, 29, 115896; c) A. Fu, R. Tang, J. Hardie, M. E. Farkas, V. M. Rotello, *Bioconjug Chem* **2014**, 25, 1602; d) S. F. Dowdy, *Nat. Biotechnol.* **2017**, 35, 222.
- [2] A. R. K. Kumar, Y. Shou, B. Chan, K. L. A. A. Tay, *Adv. Mater.* **2021**, 33, 2007421.
- [3] a) M. P. Stewart, A. Sharei, X. Ding, G. Sahay, R. Langer, K. F. Jensen, *Nature* **2016**, 538, 183; b) J. He, L. Yu, X. Lin, X. Liu, Y. Zhang, F. Yang, W. Deng, *Viruses* **2022**, 14; c) D. Morshedi Rad, M. Alsadat Rad, S. Razavi Bazaz, N. Kashaninejad, D. Jin, M. Ebrahimi Warkiani, *Adv. Mater.* **2021**, 33, 2005363; d) F. Scaletti, J. Hardie, Y. W. Lee, D. C. Luther, M. Ray, V. M. Rotello, *Chem. Soc. Rev.* **2018**, 47, 3421; e) Y. J. Yang, D. J. Mai, T. J. Dursch, B. D. Olsen, *Biomacromolecules* **2018**, 19, 3905; f) A. Namvar, A. Bolhassani, N. Khairkhan, F. Motevalli, *Biopolymers* **2015**, 103, 363.
- [4] a) R. T. Stiepel, E. Duggan, C. J. Batty, K. M. Ainslie, *Bioeng. Transl. Med.* **2022**; b) S. Pottanam Chali, B. J. Ravoo, *Angew Chem Int Ed Engl* **2020**, 59, 2962; c) G. Gunkel-Grabole, S. Sigg, M. Lomora, S. Lorcher, C. G. Palivan, W. P. Meier, *Biomater. Sci.* **2015**, 3, 25.
- [5] a) S. Du, S. S. Liew, L. Li, S. Q. Yao, *J. Am. Chem. Soc.* **2018**, 140, 15986; b) J. Gilleron, W. Querbes, A. Zeigerer, A. Borodovsky, G. Marsico, U. Schubert, K. Manygoats, S. Seifert, C. Andree, M. Stoter,

- H. Epstein-Barash, L. Zhang, V. Kotliansky, K. Fitzgerald, E. Fava, M. Bickle, Y. Kalaidzidis, A. Akinc, M. Maier, M. Zerial, *Nat. Biotechnol.* **2013**, *31*, 638; c) R. Goswami, T. Jeon, H. Nagaraj, S. Zhai, V. M. Rotello, *Trends Pharmacol. Sci.* **2020**, *41*, 743.
- [6] a) F. Wang, Y. Wang, X. Zhang, W. Zhang, S. Guo, F. Jin, *J Control Release* **2014**, *174*, 126; b) G. Guidotti, L. Brambilla, D. Rossi, *Trends Pharmacol. Sci.* **2017**, *38*, 406; c) Y. Takeuchi, K. Ushimaru, K. Kaneda, C. Maruyama, T. Ito, K. Yamanaka, Y. Ogasawara, H. Katano, Y. Kato, T. Dairi, Y. Hamano, *Commun Biol* **2022**, *5*, 1132.
- [7] T. Takeuchi, S. Futaki, *Chem. Pharm. Bull.* **2016**, *64*, 1431.
- [8] P. G. Dougherty, A. Sahni, D. Pei, *Chem. Rev.* **2019**, *119*, 10241.
- [9] Y. Sun, S. Y. Lau, Z. W. Lim, S. C. Chang, F. Ghadessy, A. Partridge, A. Miserez, *Nat. Chem.* **2022**.
- [10] J. Liu, E. Spruijt, A. Miserez, R. Langer, *Nat. Rev. Mater.* **2023**, *1*.
- [11] T. Lu, S. Liese, L. Schoenmakers, C. A. Weber, H. Suzuki, W. T. S. Huck, E. Spruijt, *J. Am. Chem. Soc.* **2022**, *144*, 13451.
- [12] a) H. Yokoo, M. Oba, S. Uchida, *Pharmaceutics* **2021**, *14*, 78; b) B. R. Liu, S. H. Chiou, Y. W. Huang, H. J. Lee, *Membranes* **2022**, *12*; c) S. G. Patel, E. J. Sayers, L. He, R. Narayan, T. L. Williams, E. M. Mills, R. K. Allemann, L. Y. P. Luk, A. T. Jones, Y. H. Tsai, *Sci. Rep.* **2019**, *9*, 6298.
- [13] G. Tünnemann, G. Ter-Avetisyan, R. M. Martin, M. Stöckl, A. Herrmann, M. C. Cardoso, *J Pept Sci* **2008**, *14*, 469.
- [14] Y. Lin, H. Jing, Z. Liu, J. Chen, D. Liang, *Langmuir* **2020**, *36*, 1709.
- [15] C. Paganini, U. Capasso Palmiero, S. Picciotto, A. Molinelli, I. Porello, G. Adamo, M. Manno, A. Bongiovanni, P. Arosio, *Small* **2022**, 2204736.
- [16] a) T. Lu, E. Spruijt, *J. Am. Chem. Soc.* **2020**, *142*, 2905; b) T. Lu, K. K. Nakashima, E. Spruijt, *The journal of physical chemistry. B* **2021**, *125*, 3080.
- [17] Y. Hong, S. Najafi, T. Casey, J. E. Shea, S. I. Han, D. S. Hwang, *Nat. Commun.* **2022**, *13*, 7326.
- [18] W. C. Su, D. L. Gettel, M. Chabanon, P. Rangamani, A. N. Parikh, *J. Am. Chem. Soc.* **2018**, *140*, 691.
- [19] a) P. Nakhaei, R. Margiana, D. O. Bokov, W. K. Abdelbasset, M. A. Jadidi Kouhbanani, R. S. Varma, F. Marofi, M. Jarahian, N. Beheshtkhoo, *Front Bioeng Biotechnol* **2021**, *9*, 705886; b) E. Rideau, R. Dimova, P. Schwillie, F. R. Wurm, K. Landfester, *Chem. Soc. Rev.* **2018**, *47*, 8572.